

A New Design of Single-Phase Current Source PV Inverter with Load Variation Using Lab View Platform

Abdel-Karim Daud¹, Sameer Khader²

^{1,2}*Palestine Polytechnic University, Department of Electrical Engineering, Hebron, Palestine*

Abstract- This paper proposes a new circuit configuration and a control scheme for a single-phase current source inverter with load variation. Different operational modes of this inverter are depicted. A sine-triangular wave pulse width modulation SPWM technique is applied. The inverter is implemented using a single boost switch, an H-bridge inverter, and a CLC output filter. The switching angle of the inverter is optimized through PWM shifting angle. The triggering signals of the each of the power switch are generated from comparing sinusoidal wave as the reference of 50Hz frequency with triangular wave as carrier signal of 40 MHz frequency. Waveform analysis has been detailed to obtain the harmonic amplitude of the output current. This paper reveals that proposed single phase current source inverter operates with different loads generates variable percentages of THD with constant modulation index of 0.9 and very high frequency modulation ratio according to carrier signal frequency. The simulations have been done in LabVIEW software to showcase the harmonic spectrum, output voltages and currents waveforms. Discrete simulated values of proposed CSI parameters are processed and converted into continuous functions using Matlab Platform. From the simulated results, the output current THD is around 1.72%. In addition, the output power factor over of 99% and a maximum efficiency over 95% are obtained.

Keywords- Current Source Inverter, Sinusoidal Pulse Width Modulated (SPWM), Harmonic Decomposition, LabVIEW Simulation, MATLAB Simulation & Multisim Simulation.

I. INTRODUCTION

In recent years, solar power generation systems are widely used in response to the fast grows and high demands of electrical energy. Due to the environmental advantages, solar power generation systems are often applied in the housing and industries areas. One of key components of the solar power systems is the photovoltaic (PV) inverter [1]-[6]. Grid-connected inverters for renewable energy systems are exponentially increasing and developing rapidly. Most renewable energy resources such as solar energy have a significant drawback, since their produced power is unregulated and discontinuous. In order to convert discontinuous output power from renewable energy resources to useful grid voltages, grid-connected inverters are used. Various converter topologies and inverter schemes have been proposed for single-phase grid-connected inverters. Generally, Inverters can be categorized into two types such as single phase inverters and three phase inverters. Inverters are also classified as voltage source inverters where the small or negligible reactor is connected in series with voltage supply and current source inverter where high inductance is connected in series with voltage supply [7],[8].

Inverters can be subdivided into two namely: conventional inverters and multilevel inverters. Thus, conventional inverter has a maximum of two output voltage or current level, which is associated with high output harmonic content with less number of power switches. On the other hand, multilevel inverter configuration has a minimum of three output voltage level with reduced harmonic content and increased number of switches [7]-[10].

The dc voltage electricity sources available such as batteries, solar panels or fuel cells are converted to dc current source by connecting in series a large inductance to establish current flow in the circuit [8]. Figure 1 shows a block diagram of photovoltaic (PV) system with CSI.

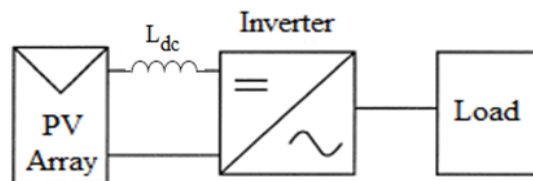


Figure 1. Block diagram of PV system with CSI

Because of unavailability of feedback diodes, the CSI is short circuit proof and cannot withstand high reverse voltage and therefore needs series diode. Although, current source inverters (CSIs) feature increasing attention

because of their advantages, like inherent current short-circuit proof, simplified filtering requirement, boosting-up capability, and low THD for their output voltage.

Pulse width modulation (PWM) inverter techniques are motivated and developed to control the output AC voltage as well as reduce the harmonics by implementing multiple switching within the inverter with a constant dc input voltage. There a variety of PWM techniques: sinusoidal PWM (SPWM), hysteresis band current control PWM, random PWM, space-vector PWM, etc. The SPWM technique is very popular for industrial inverters [9]-[13].

The circuit schematic in figure 2 depicts a conventional single-phase full bridge current source inverter which consists of a large series inductance and a traditional current-source inverter with load. This paper proposes a new single-stage current source inverter with load variation. The proposed inverter is constructed based on a current source inverter with a single boost switch, an H-bridge inverter, and a CLC output filter as shown in figure 3. A sine-triangular wave pulse width modulations PWM technique is applied for controlling this inverter. The proposed topology and its operation are described. Performance of the proposed inverter along with its controller is predicted by simulation study using LabVIEW software. The proposed technique offers excellent performance with simple implementation without aggressive computational burden.

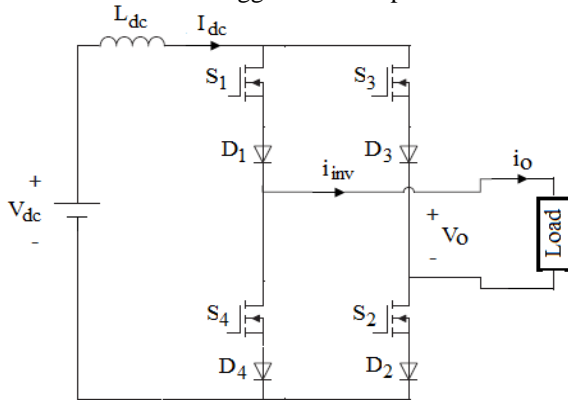


Figure 2. The conventional PV inverter.

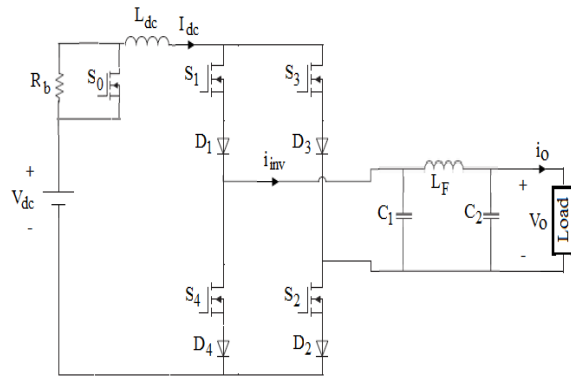


Figure 3. Circuit structure of the proposed PV inverter

II. SYSTEM DESCRIPTION

The current source inverters (CSI) in figures 2 or 3 don't usually have anti parallel diodes connected across the unidirectional switches because for a given switching state the active switch current flows in only one direction [13],[14]. The proposed CSI is connected to the load via CLC filter (C1, C2, L_F) as shown in figure3. Five power switches (S₀, S₁-S₄) and four series diodes (D₁-D₄) forms the CSI power components. The switch S₀ is used to limit the dc source surge current according to its rated value, through connecting and disconnecting of the resistance R_b during active (S₀=1) and inactive (S₀=0) switching mode. A smoothing inductor (L_{dc}) is used for minimizing the DC-link current ripples. The DC source (V_{dc}) represents a battery or any renewable energy source with its associate DC/DC converter as input to the CSI. The single phase CSI's operation can be divided into four switching states, as illustrated in table 1, figure 4 and figure 5a-d. In table 1, ON-state is depicted by 1 whereas OFF-state is depicted by 0.

Table 1. Output current switching pattern.

Modes	S ₀	S ₁	S ₂	S ₃	S ₄	i _o (A)
1	1	1	1	0	0	I _{dc}
2	0	1	0	0	1	0
3	1	0	0	1	1	- I _{dc}
4	0	0	1	1	0	0

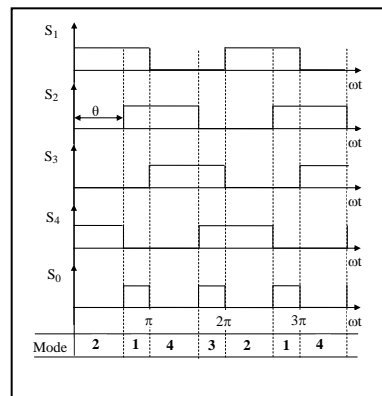


Figure4. Triggering signals for power switches.

From figure 4, the output parameters of CSI are dependent on the phase shift θ° . By regulating the control shift angle θ° , one can regulate the output parameters. During operation mode 1 (figure5 a), the power switches S_0, S_1 and S_2 are ON and other power switches i.e. S_3 and S_4 are off. Thus I_{dc} flow permits positive current flow in the circuit. Therefore, it is observed that inductor current, I_{dc} is equal to the load current, I_0 . In operation mode 2 (figure5 b), the switches S_1 and S_4 are turned ON, switches S_0, S_2 and S_3 are turned OFF, and the load receives the current during discharging of inductor L_F . In this case, current source inverter I_{dc} is termed short circuit proof and therefore, the reactor L_{dc} is charged by the circuit current. The series resistance R_b limits the short circuit current. Therefore, it is observed that inductor current, I_{dc} is not equal to the load current, I_0 . In operation mode 3 (figure5 c), the switches S_1 and S_2 are turned OFF, switches S_0, S_3 and S_4 are turned ON. Thus I_{dc} is allowed to flow through the load via the three ON switches. This flow permits negative current flow in the circuit. Therefore, it is observed that inductor current, I_{dc} is equal to the negative load current, I_0 . In mode operation 4 (figure5 d), the switches S_0, S_1 and S_4 are turned OFF, switches S_3 and S_2 are turned ON. It is similar to operation mode 2, but the load current flows in opposite direction.

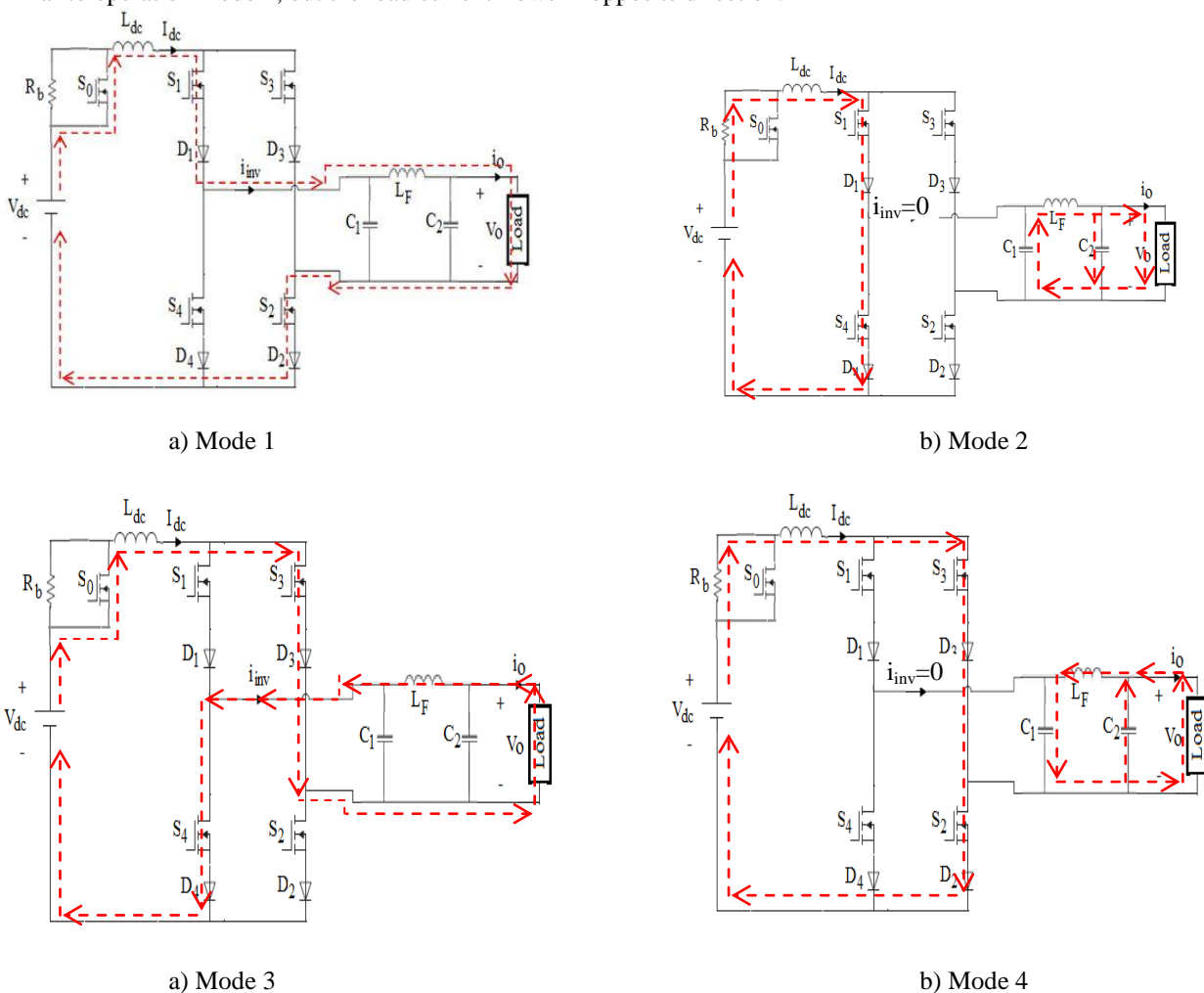


Figure 5. Operation modes of the proposed inverter.

III. SINUSOIDAL PULSE WIDTH MODULATION

Sinusoidal Pulse Width Modulation (SPWM) technology is used for controlling of the proposed inverter. In this modulation technique are multiple numbers of output pulse per half cycle and pulses are of different width. The width of each pulse is varying in proportion to the amplitude of a sine wave evaluated at the center of the same pulse. The gating signals are generated by comparing a sinusoidal reference with a high frequency triangular signal. The principle of the generation of the SPWM signal is depicted by figure 6. Modulation signal v_m is a sinusoidal signal with a frequency of 50 Hz rather than a DC constant signal. The high-frequency triangular carrier signal v_c

has a frequency of 40 MHz, which can be generated by using LabVIEW software (FPGA – PWM). Therefore, the frequency modulation ratio is very high with 20000 ticks per cycle [15],[16].

Usually regulation the CSI performances is realized by changing either the amplitude modulation index MA or the frequency modulation ratio MF in order to achieve pure sinusoidal and ripple free output voltage and current at given configuration of the filter topology. Furthermore, the switching shift angle θ° should be optimized to get the best CSI performances for high efficiency.

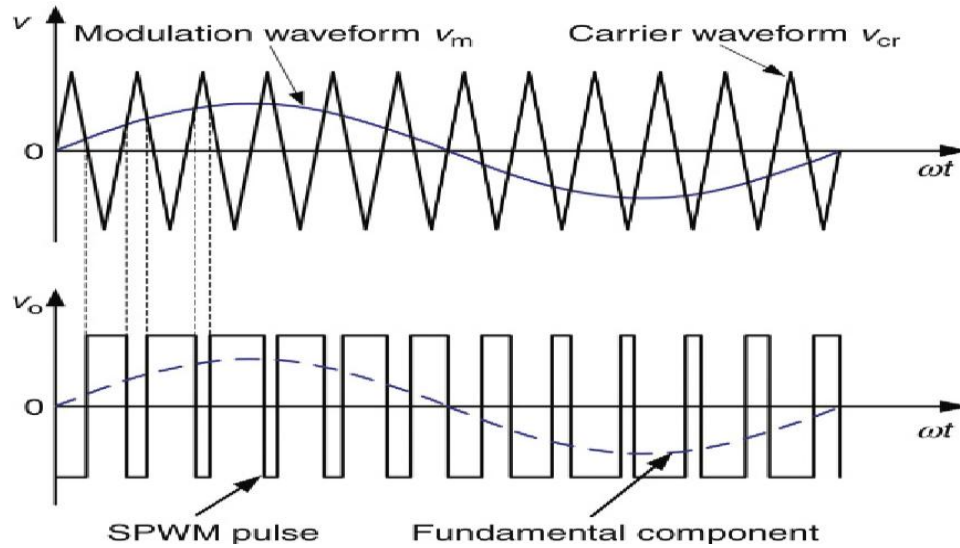


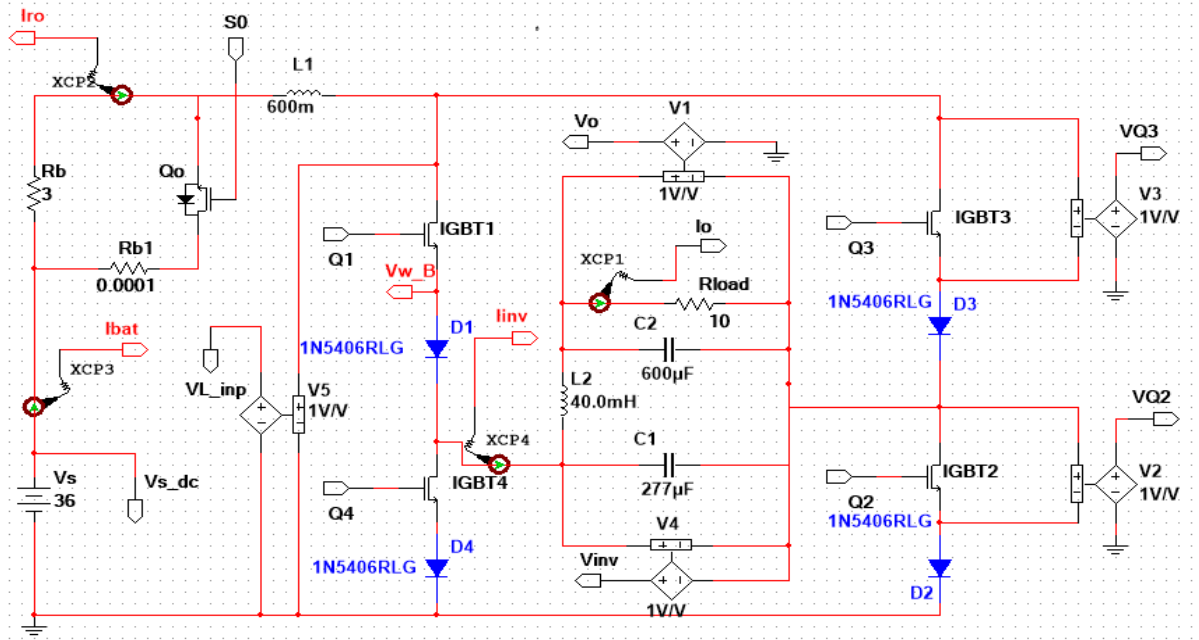
Figure 6. Sinusoidal PWM pulses.

IV. SIMULATION RESULTS UNDER DIFFERENT LOADS

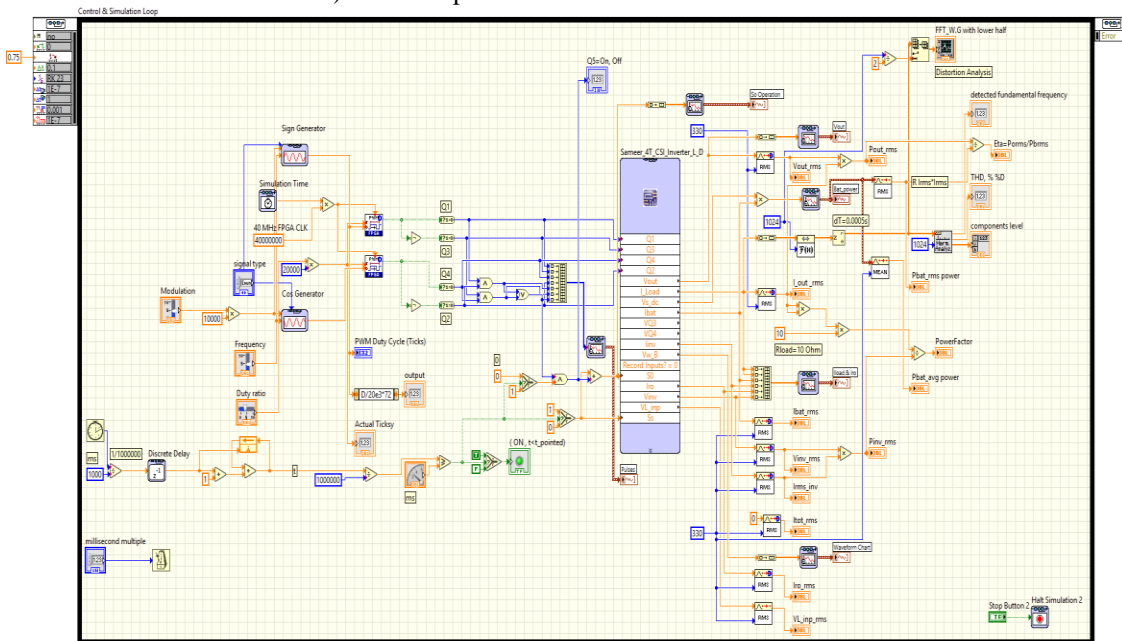
The proposed CSI mentioned circuit configuration is simulated using Multisim simulation package [15] in LabVIEW platform [16], as shown in figure 7, where the load and inverter data are stated in table 2.

Table 2. PWM and Load Specifications.

PWM Generation		Load Data	
Type	FPGA-SPWM	R	10Ω
Carrier frequency	40 MHz	L	20mH
Reference frequency	50Hz	C	600uF
Amplitude modulation index MA	0.9		
Pulses per period, Ticks	20000		
Filter data		CSI data	
C1	600uF	Rb	3 Ω
C2	277uF	Ldc	600mH
Lf	40mH	Vdc	36V
		D1-D4	1N5406RLG
		Q1-Q5 or (S1-S4& S0)	Universal



a) Multisim platform for the simulated model.



b) LabVIEW platform for the simulated model

Figure7. Simulation platforms of the proposed model.

The conducted simulation results are obtained for the both circuits in figures 2 and 3. The SPWM switching patterns are generated by comparing one triangular carrier, at switching frequency of 40MHz against a sinusoidal reference wave, a fundamental frequency of 50Hz. The simulation is obtained at optimized switching angle θ , which will be declared for the proposed CSI circuit in figure3 as follows.

In order to define the optimized PWM shift angle θ , the circuit voltage and currents are simulated for whole range of this angle ($0 \leq \theta \leq 180^\circ$) for resistive load. Figure 8 illustrates the load current with discrete and continuous simulated results called splined or fitted function obtained by using Matlab platform [17], where it can be noted that there is complete coincidence between two curves, furthermore significant load current can be drawn at large values of θ .

Figure 9 illustrates different currents of load I_o , inverter I_{inv} and dc source I_{dc} of proposed CSI circuits versus the shifting angle θ . At a large value of the shifting angle, the source current is reduced to the value, which is closed with the load current's value that is maintained unchanged at these values. Furthermore, the source current approaches high values at small values of θ .

Fig.10 illustrates the system efficiency versus shifting angle θ . From these figures it can be stated that the inverter circuit applying combination of PWM switching and continuous switching of S_0 realizes low input current and high efficiency at given load and shifting angle θ . Referring to figure 9 and 10, these results occur at optimized switching angle about $\theta_{opt} = 168^\circ$, where the CSI inverter approaches the maximum value of the efficiency and minimum input current at fixed loading current. The same results can be obtained, by changing the conditions of S_0 in the proposed CSI circuit. The optimized angle $\theta_{opt} = 168^\circ$ is applied for simulation of the CSI circuits in figures 2 and 3.

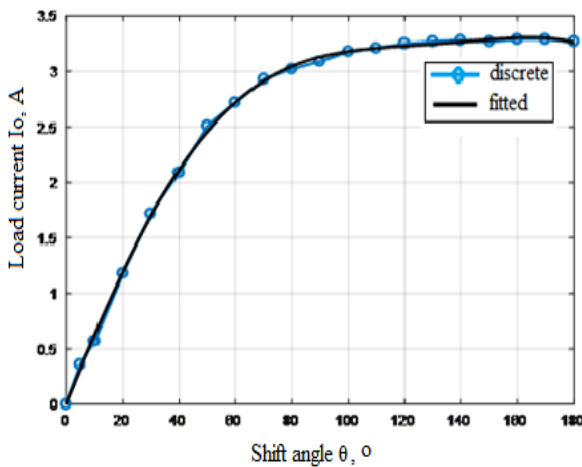


Figure 8. Load current obtained splined function.

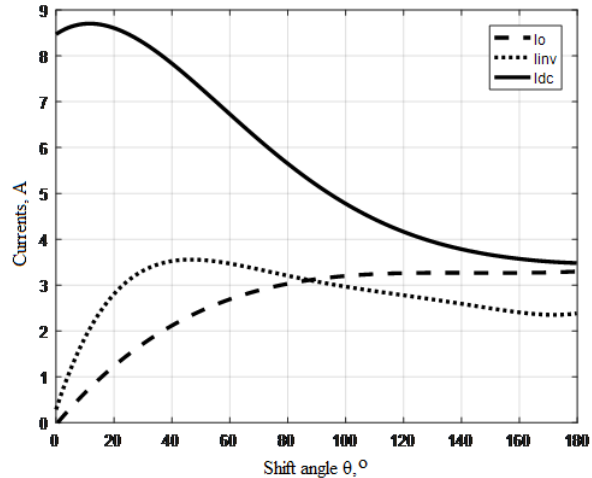


Figure 9. Circuit currents at various PWM shift angle

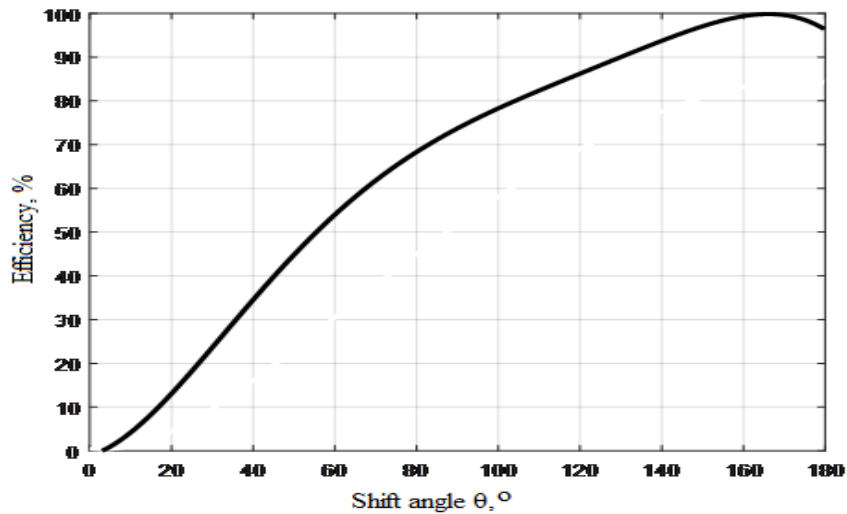


Figure 10. Efficiency versus PWM shift angle.

4.1 Simulation Results for Conventional CSI Circuit-

Refer to the conventional CSI circuit illustrates on figure 2, and the build simulation models using Multisim and LabVIEW platforms illustrated in figure 7 without filter, where the inverter is directly energized from the source without R_b and the current flows directly from the source to the load throughout the inverter having the normal operation sequence for S_1 - S_4 as illustrated on figure 4. The obtained simulation results in form of voltage and currents waveforms are displayed in figure 11 (a) and (b) respectively. Figure 11(c) displays the delivered power waveform from dc source during transient condition showing the surge power until reaching the steady state value.

It can be noticed that the dc source is stressed to high surge discharging current at the beginning of transient process, which in turn causes further heat to the all system components and on long run fast ageing. Here, the outputs current and voltage are almost in phase with high harmonic spectrum, great THD and relatively low efficiency. The result depicts output current lower than input current.

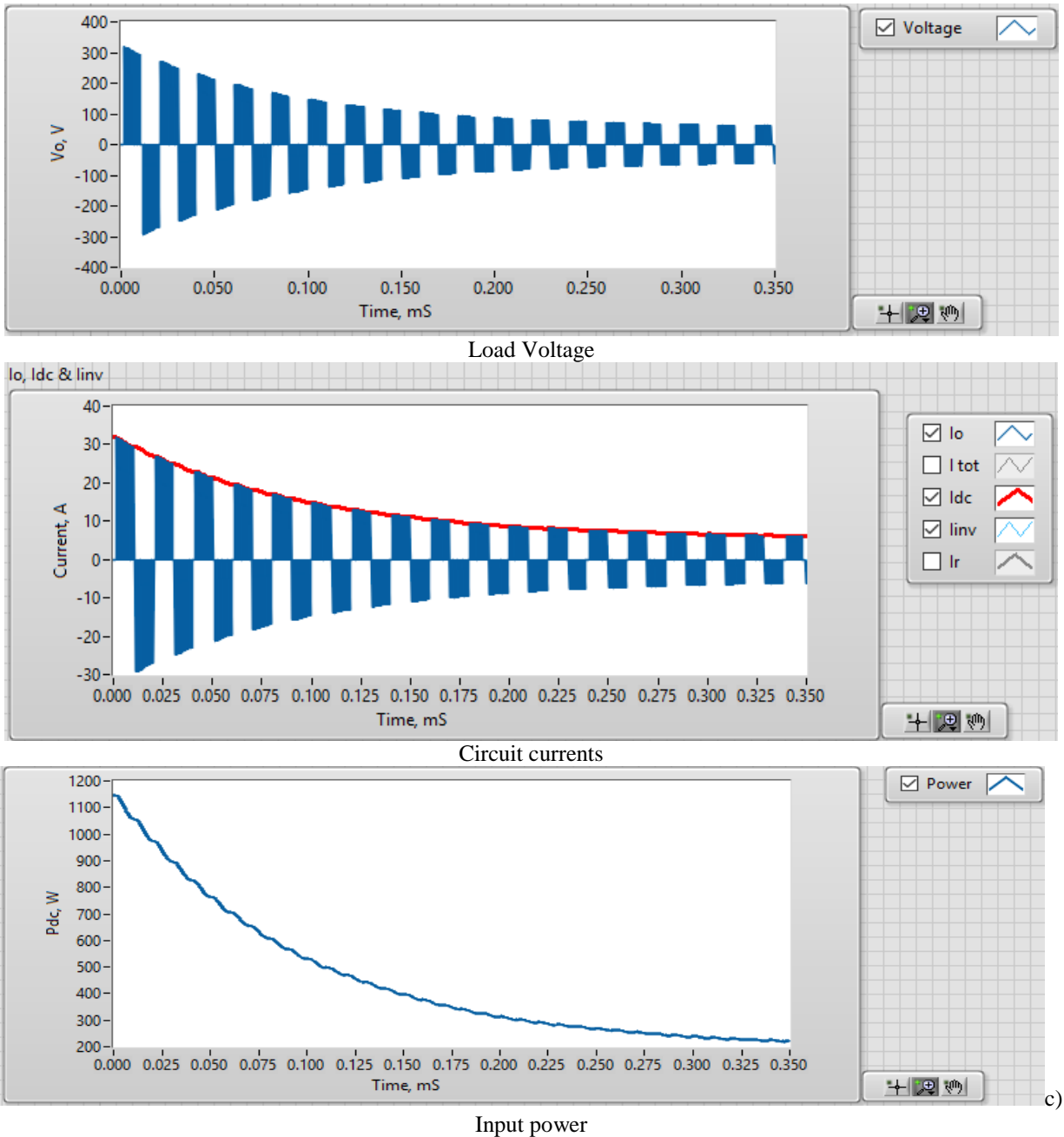


Figure 11. CSI performances of conventional circuit of figure2.

4.2 Simulation Results for Proposed CSI Circuit-

Refer to the proposed circuit illustrated on figure 3, where during CSI operation the dc source has so called boost operation cycle, when the two switches from the same arm conducted ($S1$ & $S4$) or ($S2$ & $S3$) leading to high current to flow for certain operation time, which in turn causes heavy thermal stress on the source and switching devices. One of the key factors that affect the value of this current is regulating the PWM shifting angle θ closed

between the two sinusoidal signals used to generate the PWM pulses for the two operation groups (S1& S3) and (S2& S4). To study the effect of this angle over the circuit currents two switching cases are applied with respect to the auxiliary switch S0 in order to limit the source surge current as follow:

Case A: When S0 is triggered sequentially according to the switching procedure shown in figure4 and again displayed in figure 12 (a).

Case B: During the starting process of the system,S0 is deactivated then activated according to the switching procedure shown in figure4untilthe input current comes nearly to its steady state value for suitable time t_{ss} and then S0 is activated with continuous switching signal as shown in figure 12(b).

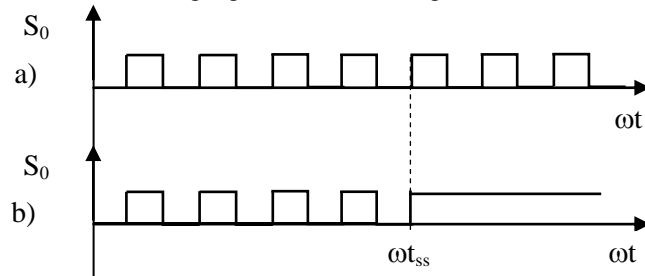
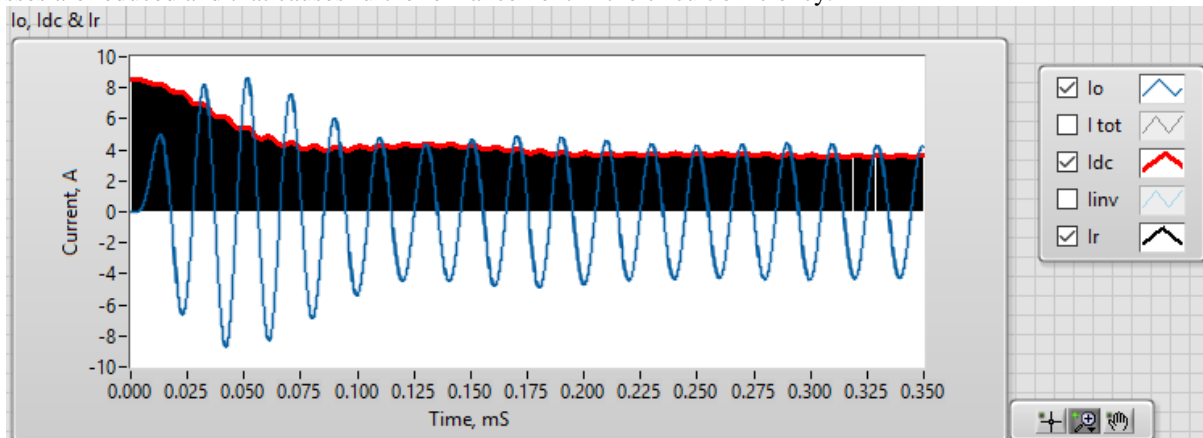


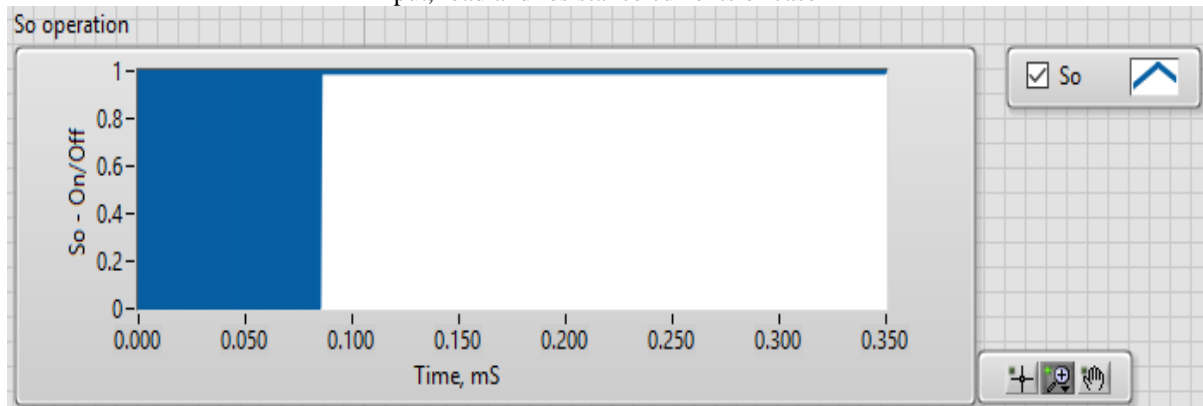
Figure 12. Conditions of switch S0 to limit the battery starting current.

Having the optimized angle into consideration, the limiting resistance current I_r and switch S0operation during transient process are displayed in figure 13, where figure 13(a) shows that while the load current has pure sinusoidal character, the limiting resistance current has high intensity of pulse sequence according to the operation mode mentioned for case A. Due to copper losses from resistance R_b , the circuit efficiency is reduced.

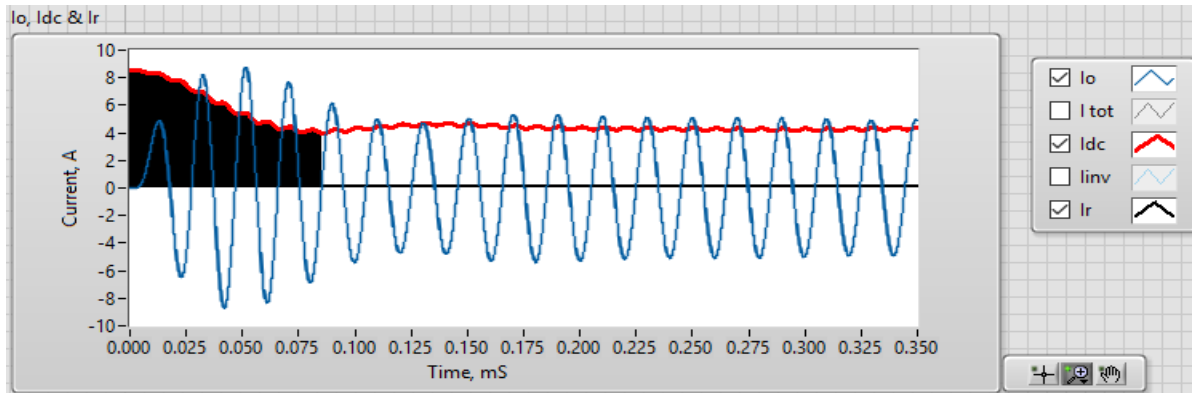
Figure 13 b) show the transient operation of switch S0 according to figure 12b), where the limiting resistance R_b is shorted by activating of S0after reaching the input current I_{dc} its steady state value as shown in figure 13c). So the transient curves of other currents (i_{inv} and i_0) are shown in figure 13b). According to the shorting of R_b , the copper losses are reduced and that causes further enhancement in the circuit efficiency.



Input, load and resistance currents of case A



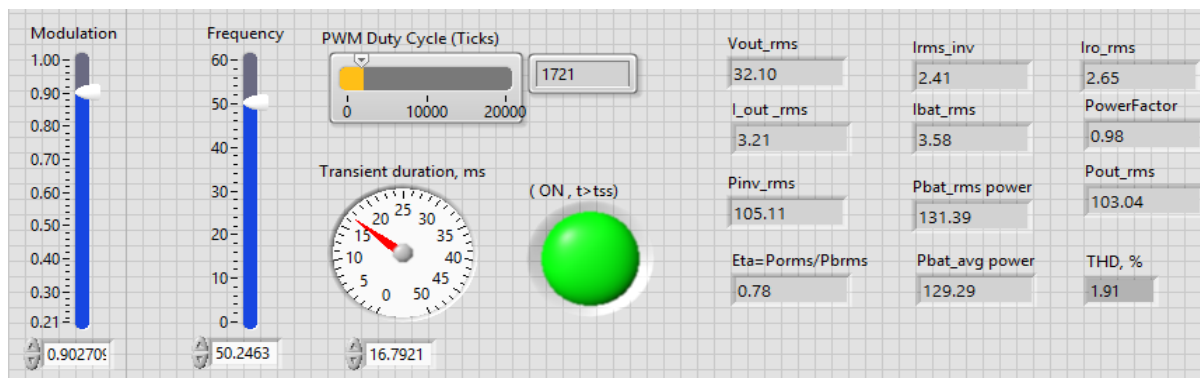
PWM operation for S0for case B



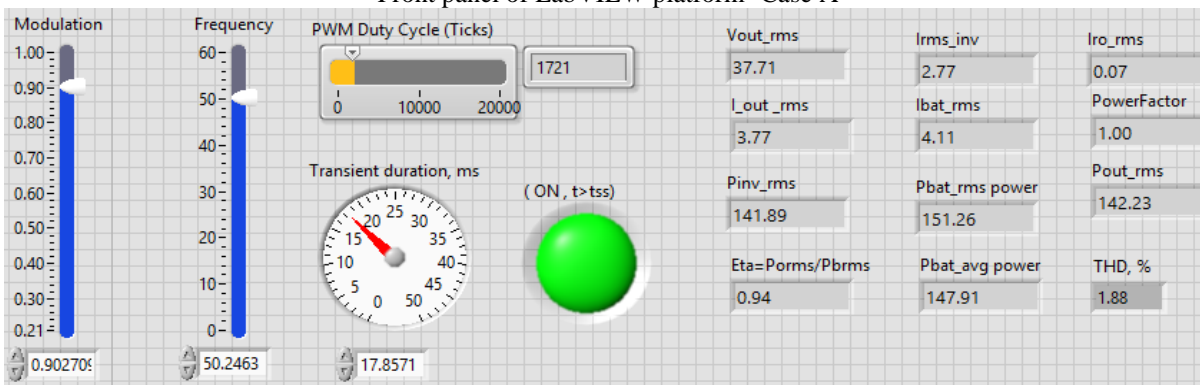
Input, load and resistance current curves for case B

Figure 13. Operation modes of boost switch S0 and related currents

Now, with this optimized angle, the system is simulated for the two cases where obtained results are displayed in figure 14 throughout LabVIEW front panel. It can be noticed from these panels that case B is characterized with better results comparing with case A with respect to the efficiency, power factor and to some extent the total harmonic distortion.



Front panel of LabVIEW platform- Case A

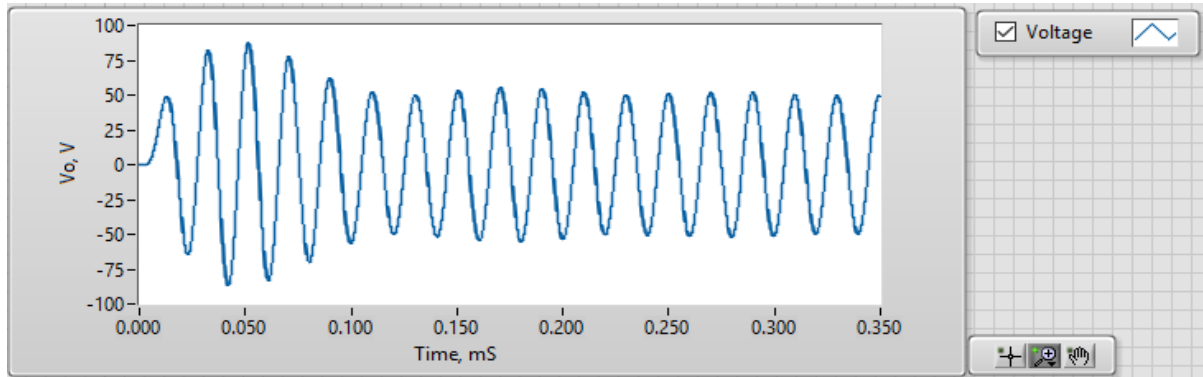


Front panel of LabVIEW platform- Case B

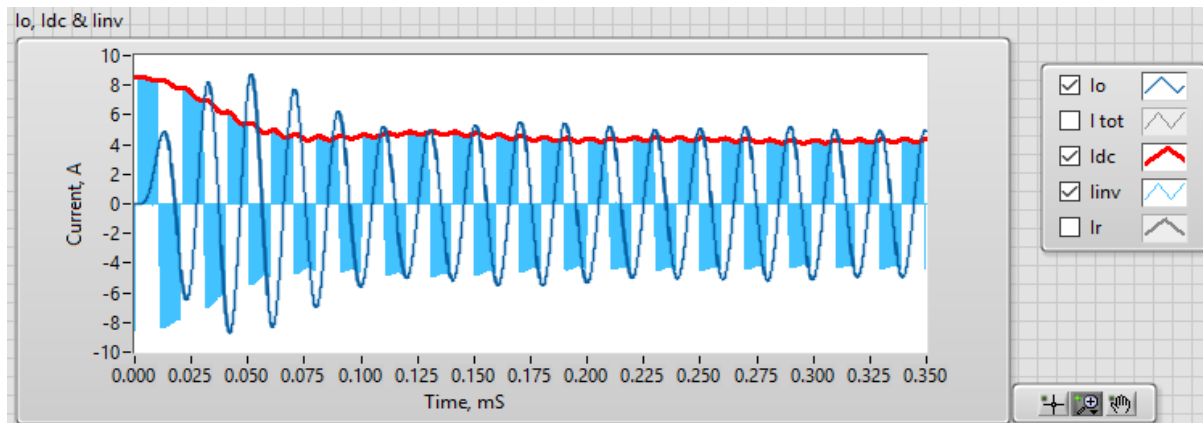
Figure 14. LabVIEW front panel for both cases.

The same results in terms of time domain for the output voltage, currents and battery power are displayed in figure 15, where the load current has peak values exceeded the input current due to filter effect on the output performance, which in turn improves the power factor, efficiency and THD.

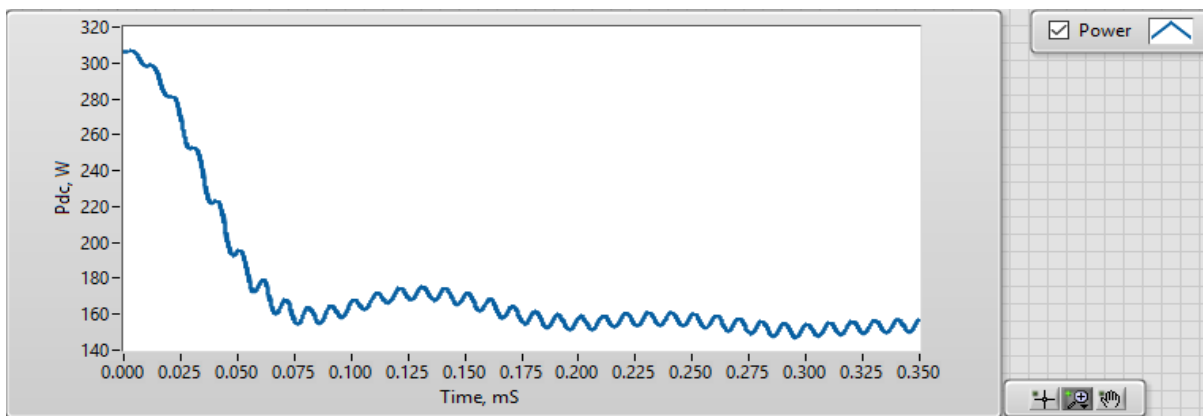
Despite the improved performance due to applying Case B control approach, but the input current has limited ripples which are converted into power fluctuation in narrow range as shown from figure 15(c).



Output voltage



Load, inverter and input currents



Input power

Figure 15. Snapshots of inverter circuit performances of case B for resistive load.

Figure 16 shows the system efficiency with respect to the load power, which is over 90% for wide range of power regulation.

4.3 The effect of R-L load

At the same optimized switching angle, by changing the load character to be R-L load with 20mH added in series with 10 Ω resistance as stated in table 2, the obtained voltage and currents are displayed in figure 17, in addition to displayed LabVIEW front panel.

Figure 17 a) presents the efficiency and power factor characteristics subjects to the output power. The output power factor is 90% at the rating power and the maximum efficiency is 94%. The total harmonics distortion (THD) of output current is 1.72%. The result depicts output current lower than input current.

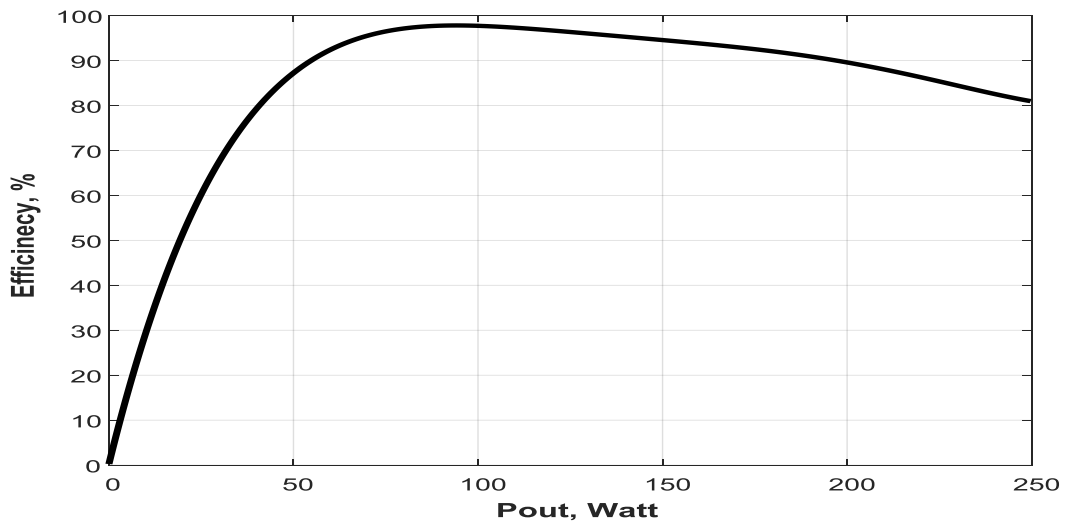
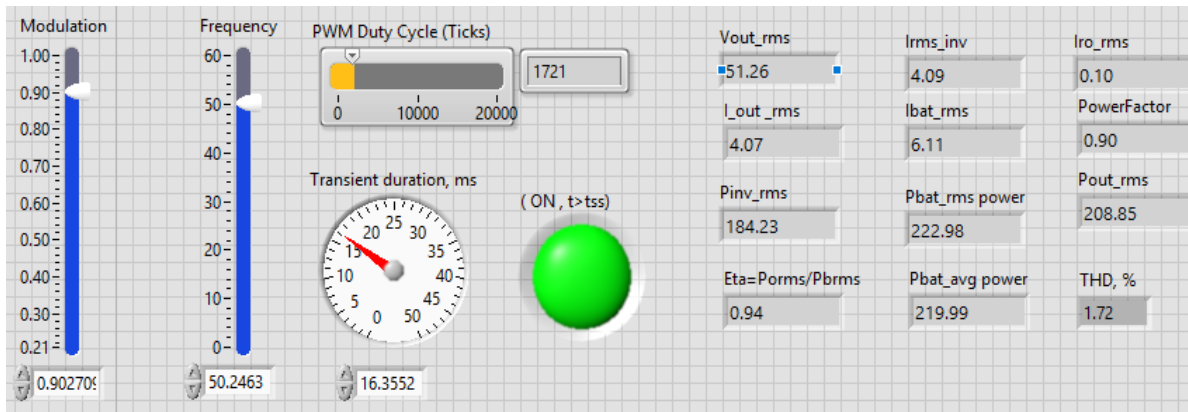
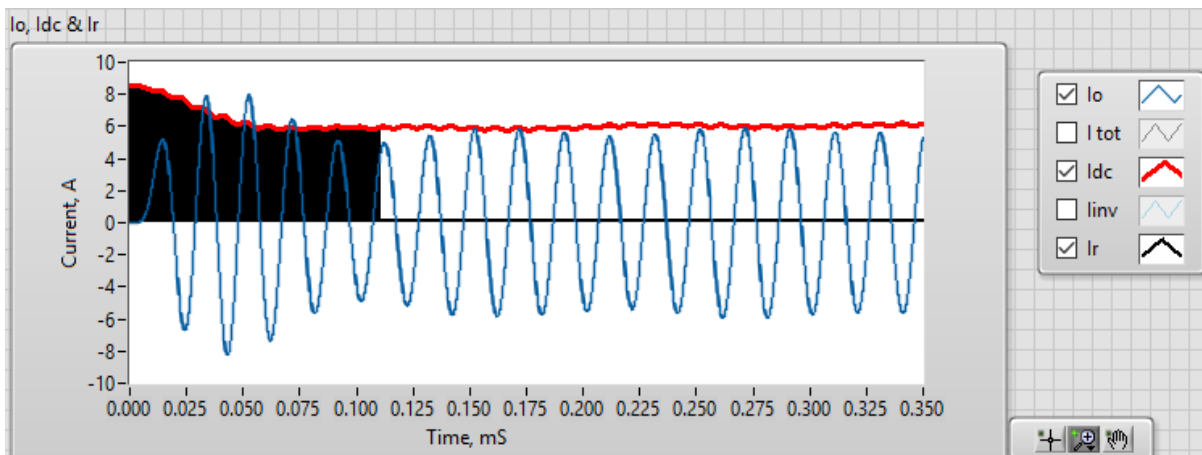


Figure 16. System efficiency for resistive load.



LabVIEW front panel for R-L load



System currents

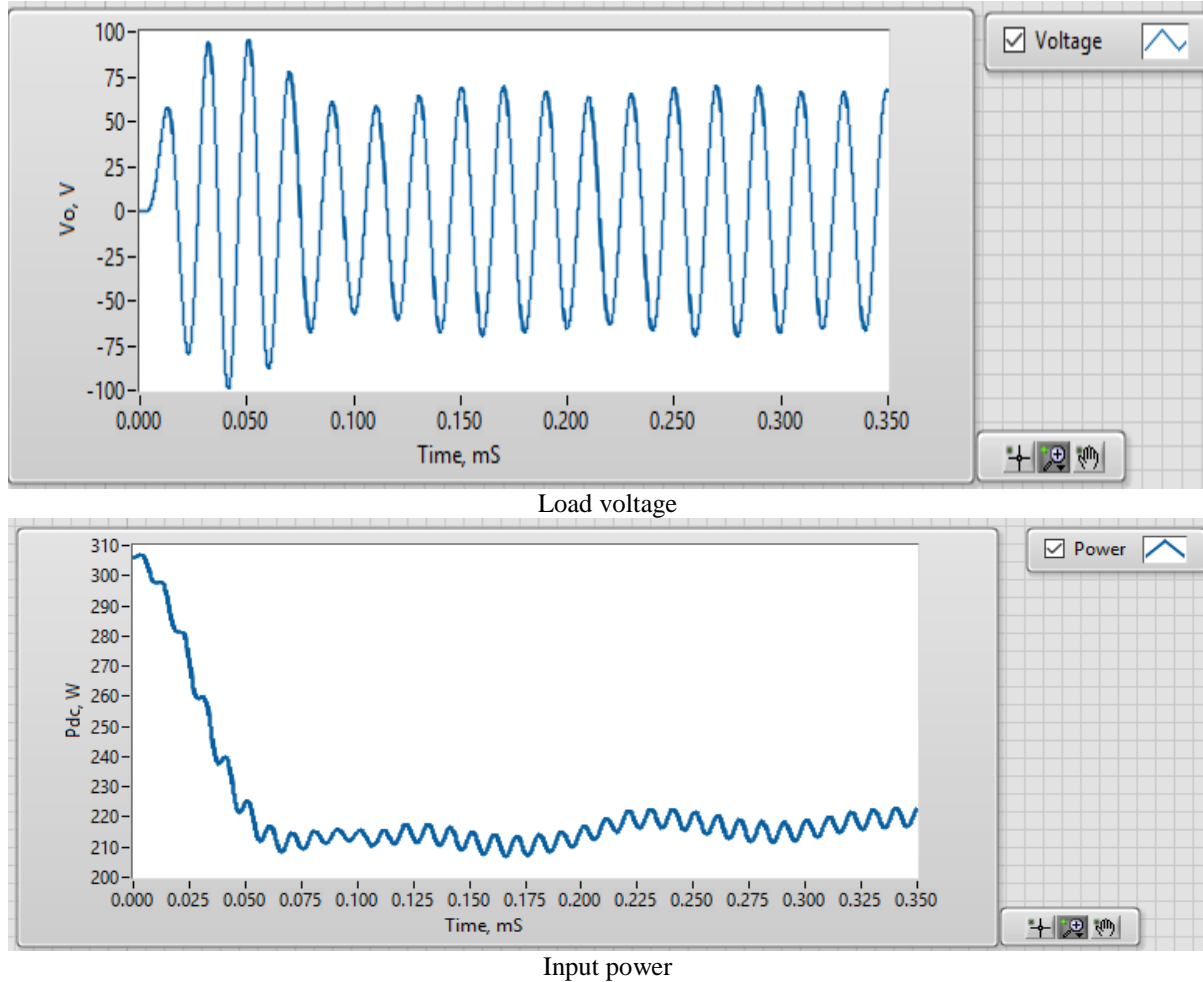
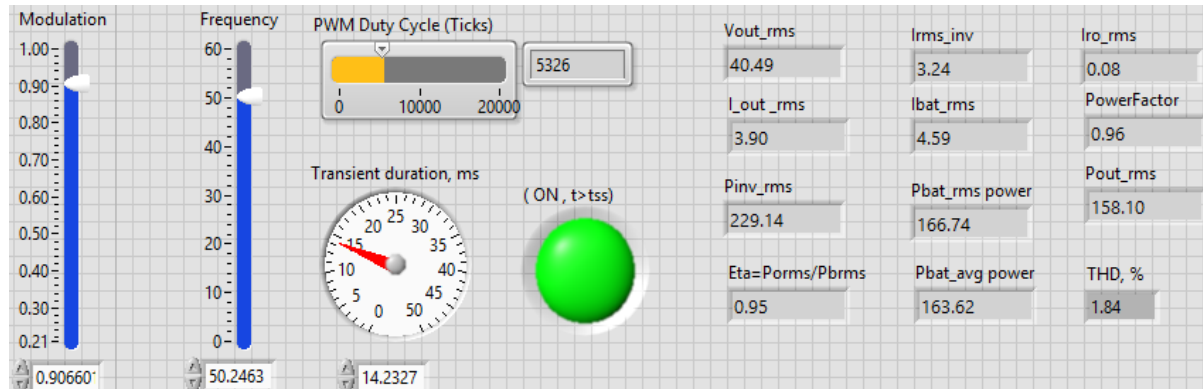


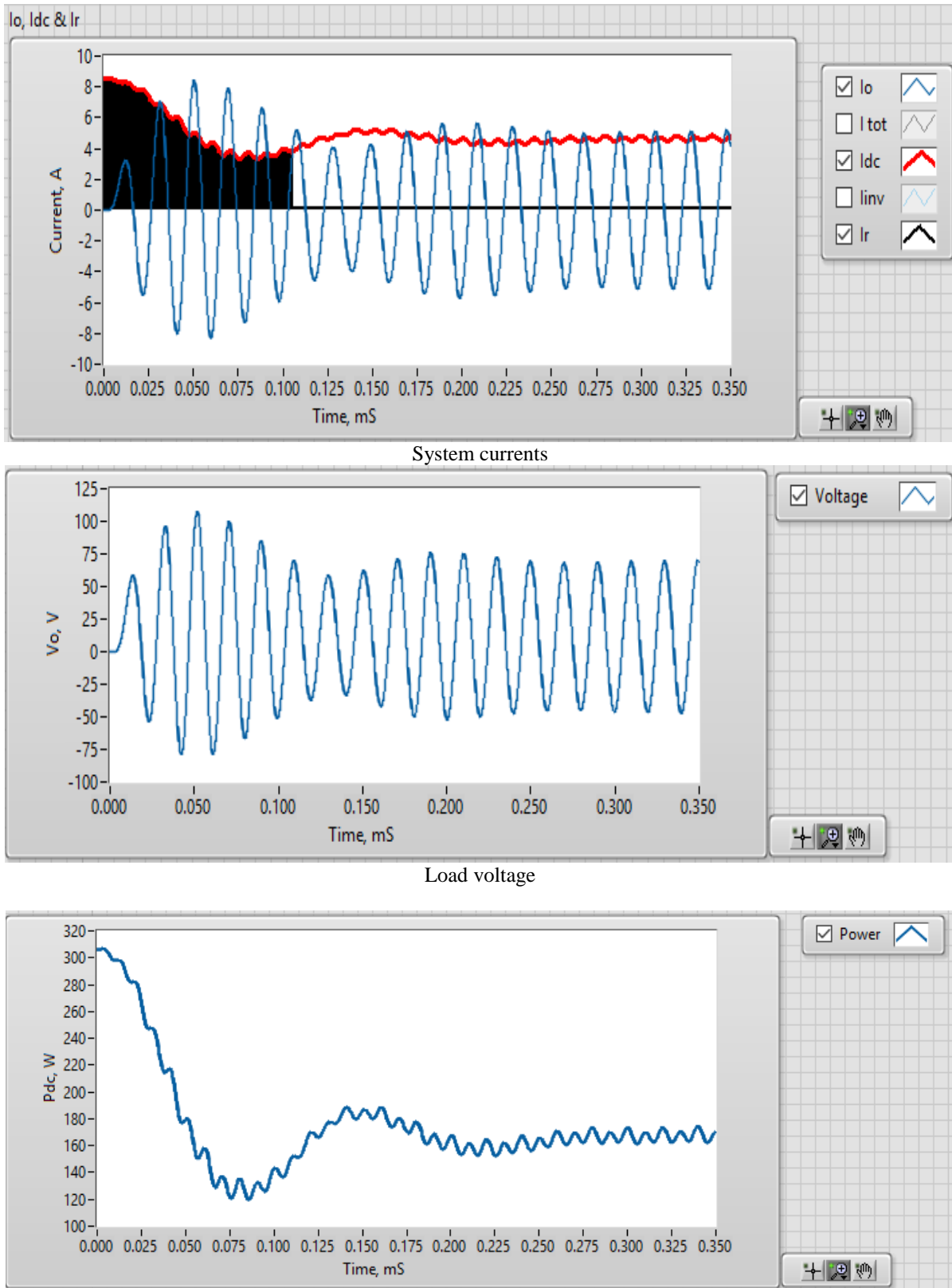
Figure 17. CSI performances of R-L load.

4.4 The effect of R–C load

At the same optimized switching angle, by changing the load character to be R-C load with 600 μ F capacitor connected in series with 10 Ω resistance as stated in table 2, the obtained voltage and currents are displayed in figure 18, in addition to displayed LabVIEW front panel. Figure 18 a) presents the efficiency and power factor characteristics subjects to the output power. The output power factor is 96% at the rating power and the maximum efficiency is about 95%. The total harmonics distortion (THD) of output current is about 1.84%.



LabVIEW front panel for R-C load.



Input power
Figure 18. CSI performances of R-C load.

V. CONCLUSIONS

This paper proposes a new circuit topology and a control scheme for a single-phase current source inverter with a single boost switch that reduces the excesses heat on all system components, where the drawn output load current has pure sinusoidal waveform. In this paper, the fundamental operations of the proposed inverter are demonstrated and simulated with optimized switching angle of 168° closed between the two sinusoidal reference signals for different loads using Lab View platform. The triggering signals of the each of the power switch are generated from comparing sinusoidal wave as the reference of 50Hz frequency with triangular wave as carrier signal of 40 MHz frequency throughout FPGA-PWM pulse generator, which gives very high frequency modulation ratio. From the simulated results, the THD for the output current falls down below 2%. The system losses are reduced significantly due to applying the new proposed switching topology. As a result of this topology and applied modulation, the output power factor approaches 0.99, and the maximum efficiency exceeds 95%.

Finally, the proposed LabVIEW module for conducting the simulation presents rugged and friendly user interface with real time interaction, processed results and interactive front panel.

VI. REFERENCES

- [1] M. Calais, J. Myrzik, T. Spoone, and V. G. Agelidis, "Inverters for single-phase grid connected photovoltaic systems-an overview," in Proc. 2002 IEEE 33rd Annual Power Electronics Specialists Conference, pESC 02, vol. 2, pp. 1995–2000, 2002.
- [2] S. Kjaer and J. Pedersen, "A review of single-phase grid-connected inverters for photo-voltaic modules," IEEE Trans. Ind. Ap., vol. 41, no. 5, pp. 1292-1306, 2005.
- [3] S. Khader, A.K. Daud, "PHOTOVOLTAIC-GRID INTEGRATED SYSTEM", First International Conference on Renewable Energies and Vehicular Technology (REVET 2012) Nabeul, Tunisia, pp. 60-65, 2012.
- [4] A. K. Daud, M. Mahmoud, "Solar powered induction motor-driven water pump operating on a desert", Renewable Energy, April 2005, Vol. 30, pp. 701-714.
- [5] A. K.Daud, M. Ismail, W. Kukhun, M. Mahmoud, "Simulation of a Hybrid Power System Consisting of Wind Turbine, PV, Storage Battery and Diesel Generator: Design, Optimization and Economical Evaluation", International Journal of Energy Engineering (IJEE) Vol.1, No.1, pp.56-61, 2011.
- [6] S. Khader, A. K. Daud, "PV-Grid Tie System Energizing Water Pump", Smart Grid and Renewable Energy (SGRE), ISSN Print: 2151-481X, Vol. 4, No. 5, pp. 409-418, 2013.
- [7] M. H. Rashid, Power Electronics, Devices, Circuits, and Applications. 4th edition, Pearson Education Limited 2014.
- [8] M. H. Rashid, Electric Renewable Energy Systems. Academic Press of Elsevier 2016.
- [9] H. Komurcugil, "Steady-State Analysis and Passivity-Based Control of Single-Phase PWM Current-Source Inverters," Industrial Electronics, IEEE Transactions on , vol.57, no.3, pp.1026-1030, 2010.
- [10] R.T.H. Li, H. S.H. Chung, T.K.M. Chan, "An Active Modulation Technique for Single-Phase Grid-Connected CSI," Power Electronics, IEEE Transactions on, vol.22, no.4, pp.1373-1382, July 2007
- [11] Masri and P. W. Chan, "Design and development of a dc-dc Boost converter with constant output voltage", IEEE, International conference on Intelligent and Advanced systems (ICIAS), June 2010.
- [12] A. Ponniran and A. F. Said., "DC-DC Boost Converter Design for Solar Electric System", International conference on Instrumentation, Control and Automation, October 20-22 (ICA 2009) Bandung.
- [13] R . Arulmurugan, N.V. Suthanthira," Optimal Design of DC to DC Boost Converter with Closed Loop Control PID Mechanism for High Voltage Photovoltaic Application ", International Journal of Power Electronics and Drive System (IJPEDS) Vol.2, No.4, pp. 434-444, December 2012.
- [14] A. Nami, A. Ghosh, and F. Blaabjerg, "A hybrid cascade converter topology with series-connected symmetrical and asymmetrical diode-clamped H-Bridge cells", IEEE Trans. Power Electron, vol. 26, no. 1, 51–65, Jan. 2011.
- [15] Multisim Simulation Platform, 14.1 ed., <http://www.ni.com/en-us/multisim/14.1>.
- [16] LabVIEW Simulation Platform, 16 ed., <http://www.ni.com/en-us/shop/labview>.
- [17] Matlab/Simulink User's Guide , 2016, www.mathwork.com